Influence of geometry on hydrodynamic focusing and long-range fluid behavior in PDMS microfluidic chips

Kunstmann-Olsen, Casper ; Hoyland, James; Rubahn, Horst-Günter

Published in:
Microfluidics and Nanofluidics

DOI:
10.1007/s10404-011-0923-1

Publication date:
2012

Document version
Early version, also known as pre-print

Citation for pulished version (APA):
Kunstmann-Olsen, C., Hoyland, J., & Rubahn, H-G. (2012). Influence of geometry on hydrodynamic focusing and long-range fluid behavior in PDMS microfluidic chips. Microfluidics and Nanofluidics, 12(5), 795-803. https://doi.org/10.1007/s10404-011-0923-1

Microfluid Nanofluid
DOI 10.1007/s10404-011-0923-1

RESEARCH PAPER

Influence of geometry on hydrodynamic focusing and long-range fluid behavior in PDMS microfluidic chips

Casper Kunstmann-Olsen · James D. Hoyland · Horst-Günter Rubahn

Received: 4 August 2011 / Accepted: 4 November 2011

Abstract Details of hydrodynamic focusing in a 2D microfluidic channel-junction are investigated experimentally and theoretically, especially the effect on the focusing width of volumetric flow ratio r between main and side channels, as well as angle θ between channels. A non-linear relationship is observed where the focus width decreases rapidly with increasing r and levels off at higher values. For the dependence on θ, results from both experiments and modeling show that an increased focusing effect is obtained as θ approaches 90°. Long-range focusing is explored along a 1 cm long channel and it is observed that in the middle section of the channel, a smaller θ induces less divergence. This effect is of importance for microfluidic systems utilizing hydrodynamic focusing in long, straight channels.

Keywords Microfluidics · Hydrodynamic focusing · PDMS chip · Junction geometry

1 Introduction

Lab-on-a-chip technology is of growing interest and is creating powerful and versatile devices for use in a wide variety of technological fields. The technology has found a wide application in biochemistry, biophysics, and medical fields such as drug delivery and screening, biological and chemical assays (Whitesides and Stroock 2001; Stone et al. 2004; Vilkner et al. 2004; Squires and Quake 2005).

One of the main advantages in these lab-on-a-chip systems is the superior and precise liquid control offered through microfluidics. Typical dimensions on the micro- and nano-scale induce steady and laminar flow which enables a wide variety of interesting possibilities, including flow cytometers for cell/particle counting and sorting (Crosland-Taylo 1953; Schrum et al. 1999; Huh et al. 2002, 2005; Lin and Lee 2003; Fu et al. 2004), cell patterning (Takayama et al. 1999), receptor-ligand assays (Regenberg et al. 2004), DNA-hybridization (Regenberg et al. 2004), DNA stretching (Wong et al. 2003), diffusion-based mixers (Knight et al. 1998; Pollack et al. 1999; Hertzog et al. 2004), micro flow switches (Blankenstein and Larsen 1998; Lee et al. 2001), bubble or droplet generators (Garstecki et al. 2004; Takeuchi et al. 2005) and micro- and nano-particle production (Martin-Banderas et al. 2005).

One of the key mechanics often utilized in these microfluidic lab-on-a-chip systems is hydrodynamic focusing. This technique was first developed by Spielman and Goren (1968) using a 3D flow setup. With miniaturization, the technique has moved down to a 2D geometry and today, using laminar flows, micrometer dimensions and volumetric flow control, hydrodynamic focusing enables precise focusing of sample liquid-streams down below 5% of their initial size (de Mello and Edel 2007). This technique is often utilized in analytical methods such as flow-cytometry or Coulter-counting (Godin et al. 2008; Zhe et al. 2007). One of the main advantages of a 2D geometry is the possibility of creating single-layer system utilizing one-step production methods such as molding, hot-embossing, ablation techniques etc. Even true 3D focusing is possible in a 2D geometry (Mao et al. 2007).

The focus of this paper is on 2D hydrodynamic focusing on a one-layer microfluidic chip, using a simple two side-channel geometry (Sundararajan et al. 2004; Howell et al. 2008). Previous investigations of similar geometry have

C. Kunstmann-Olsen (✉) · J. D. Hoyland · H.-G. Rubahn
Mads Clausen Institute, University of Southern Denmark, Alsion 2, 6400 Sønderborg, Denmark
e-mail: kunstmann@mci.sdu.dk

Published online: 08 December 2011

mainly focused on flows in high aspect-ratio T-junctions (both for gases, Gobby et al. 2001; and liquids, Yang et al. 2007) and have shown that angles between sample and side channels have some influence on concentration gradients and mixing. We explore as to how the local geometry of the channel-junction influences the hydrodynamic focusing and, consequently, the long-range divergence of the sample stream. This is of interest since many designs utilize the entire length of the channel either for flow processing or various measurements and a stable focusing is desirable.

2 Theoretical analysis

In this section, we apply current theoretical models (Lee et al. 2006) to hydrodynamic behavior in rectangular microchannels in order to predict the width of a hydrodynamically focused sample stream in a two-flow system (see Fig. 1). It is assumed that all liquids are Newtonian and have equal density (ρ) and viscosity (η). Furthermore, all channels have the same height (h) and square cross-sections ($w \cdot h$). All flows are in effect steady and laminar since the Reynolds number in the current geometry and flow conditions is between 10 and 40 depending on the flow ratio r.

From the conservation of mass it can be shown that (Lee et al. 2006)

$$f = \frac{w_f}{w_0} = \frac{1}{\gamma} \cdot \frac{Q_i}{Q_i + Q_s + Q_s} \tag{1}$$

where Q_i and Q_s are the volume flow rate of the sample and sheath, respectively, and the mean flow speed ratio $\gamma = \bar{v}_f/\bar{v}_0$ is the unknown parameter. In order to predict the width of the focused stream in Eq. 1, the velocity ratio γ must be determined. This can be done by solving the governing equation of the fluidic system, the Navier–Stokes (NS) equation via FEM modeling.

We can derive a very simplistic model for the effect of the sheath angle (θ) on f, neglecting 3D effects and velocity profiles across the flows, by considering the change in momentum undergone by the sheath fluid as it turns the corner into the exit channel. This change in momentum leads to a pressure difference between the inside and outside of the flow which is impressed on the sample flow. Further approximating the trajectory of the sheath flow as a circular arc, we can derive an estimate of this pressure via the centripetal force from the sheath fluid on a small section of the side flow as it rotates through a small angle $\delta\theta$ with radius of curvature R.

$$\frac{m\bar{v}^2}{R} = \frac{(\rho w_s h R \delta\theta)(\bar{v}_f r)^2}{R} \tag{2}$$

Here the average velocity of the sheath is found using r, the volume-flow ratio. This force is applied across an area of $hR\ \delta\theta$ and so the excess pressure exerted at the sheath-sample interface is:

$$P_{\text{centripetal}} = \frac{\rho \bar{v}_f^2 r^2 w_s}{R} \tag{3}$$

An exact expression for R is difficult to determine as the curve is not really a circle. On average, though if we consider the circle defined by using sheath-sample interface at the input and output flows as tangents (see Fig. 1, right), we obtain a radius

$$R = \frac{w_d}{\sin\theta}\left(\frac{1}{\sin\theta}\right) = \frac{w_d}{\sin^2\theta}, \tag{4}$$

which leads to a pressure of

$$P_{\text{centripetal}} = \frac{\rho \bar{v}_f^2 r^2 w_s \sin^2(\theta)}{w_d} \tag{5}$$

this pressure is in addition to the base pressure difference for the side flow, from input to output. This difference is found by simply applying Bernoulli's equation to the side flow to give

$$P_{\text{Bernoulli}} = \frac{3}{2}\rho \bar{v}_f^2 r^2 \tag{6}$$

where we have assumed f to be very small.

We can now determine the effect the total pressure $P = P_{\text{centripetal}} + P_{\text{Bernoulli}}$ on the sample. By setting the output as zero for pressure we can write Bernoulli's equation for the sample flow as:

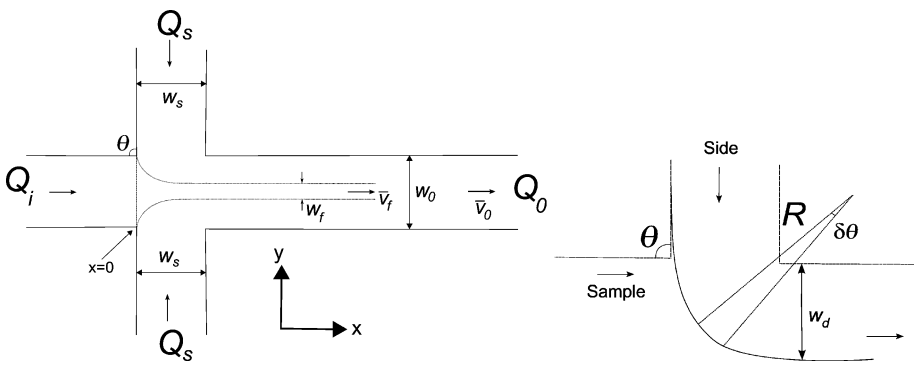

Fig. 1 *Left* schematic of symmetric 2D hydrodynamic focusing (*top view*). *Right* bending fluid stream in side flow

$$P + \frac{1}{2}\rho\bar{v}_f^2 = \frac{1}{2}\rho\frac{\bar{v}_f^2}{f^2} \tag{7}$$

And so the flow fraction can be expressed as

$$f = \sqrt{\frac{1}{1 + \frac{2P}{\rho\bar{v}_f^2}}} \tag{8}$$

Substituting these pressures (Eqs. 5 and 6) into Eq. 8 gives

$$f = \sqrt{\frac{1}{1 + 3r^2 + 2r^2\sin^2\theta}}, \tag{9}$$

which can now be used to estimate the flow fraction as a function of either angle θ or flow ratio r.

This is of course a very simple model of the flow which takes no account of 3D behavior or of the velocity profiles of the various streams. It deals only with the average inertial forces on the liquids. However, as we shall show below, the equation gives a fair approximation to the data and so is of practical use in estimating flow focusing effects in these systems.

3 Materials and methods

3.1 Chip production

The micro-channel structures are fabricated by casting poly-methyl-di-siloxane (PDMS) from an inverse structure defined by an SU8 resist on a silicon substrate. By spin-coating a thick SU8 resist (SU8-2050, MicroChem, Newton, MA, USA) on a Si-wafer, an evenly thick layer is obtained (1,500 rpm for 60 s). The wafer is subsequently pre-baked at 65°C for 5 min, and then 10 min at 90°C. For patterning the SU8 resist, a novel shadow-mask approach is used. In short, a black-and-white photo-negative is used as a substitute for a more expensive Cr-plated quartz mask, in a traditional photo lithographic process. The negative is positioned on top of the SU8 layer (in direct contact) and exposed to UV-light (220 mJ/cm^2) for 45 s (MA150 Mask Aligner, *SÜSS* MicroTec, Garching, Germany). The resist is afterwards post-baked at 65°C for 3 min, and then 10 min at 90°C. The wafer is left to cool at room temperature and then developed. This is done in a 70% SU8 developer (MicroChem, Newton, MA, USA) with 30% iso-propanol (IP), under rigid agitation. Typical development times are around 5 min. The wafer is rinsed in IP and then hard-baked for 10 min at 150°C. The thickness of the SU8-layer is measured in a profiler (Dektak 150, Brucker AXS, Madison, WI, USA) giving a thickness of 85 ± 3 μm.

The completed SU8 structure is then used as a master in a PDMS casting procedure. The Si-wafer is mounted with an O-ring in a custom-made stainless steel mold and thin (3 mm) pins are aligned with the inlet and outlet pads on the wafer. This is to facilitate flow-connectivity in the final microfluidic chip. Premixed and out-gassed PDMS (Sylgard 184, Dow Corning, Midland, MI, USA) is poured into the mold and the polymer is cured for 1 h at 100°C. This results in PDMS chips with an inverse structure from that of the SU8 master. The total channel width is measured and found to be 100 ± 5 μm. Finally, the chip is sealed using a thin (2 mm) PDMS-sheet, utilizing an oxygen plasma.

Two different mask-designs are used in this experiment, one with two perpendicular side-channels ($\theta = 90°$) and another with angled side-channels ($\theta = 67.5°$ and $\theta = 45°$). The total channel length from inlet to outlet is 3 cm. Both designs are shown in Fig. 2.

3.2 Detection

All experiments are done using deionized water in the side channels and deionized water mixed with 5% red food colour as the sample fluid. The side fluids are injected from 10 ml plastic syringes while the sample fluid is dispersed from a 1 ml plastic syringe. All three syringes are driven by two syringe pumps (Harvard Apparatus PHD2200, MA, USA). This allows for individual control of volumetric flow of side and sample flows. The chip itself is connected to the fluid-system using blunt needles that fit directly into the chip where the soft PDMS forms a tight seal.

The flow in the chip is characterized via images obtained using an optical microscope (Eclipse ME600, Nikon, Melville, NY, USA), equipped with a CCD camera

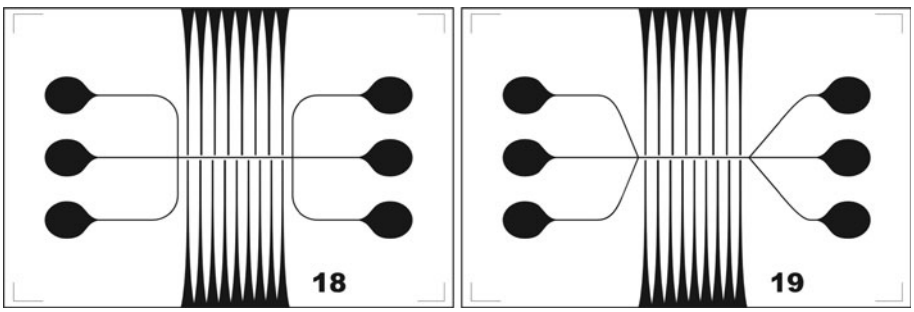

Fig. 2 Chip designs used to investigate hydrodynamic focusing. The six pads are for external connections and the tapered structures are for inserting optical fibers. *Left* perpendicular side channels ($\theta = 90°$) in both ends. *Right* angled side-channels, with $\theta = 67.5°$ and $\theta = 45°$, respectively

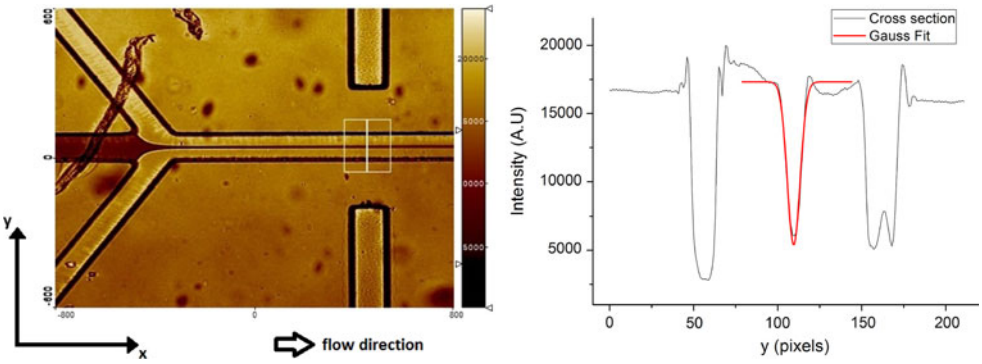

Fig. 3 *Left* microscope image showing the focused red dye and the cross-section line and average width (*white box*). *Right* plot showing x-averaged pixels cross-sectional scan and the corresponding fitted Gaussian curve. The two additional peaks are due to channel boundaries

(PL-B873-CF, PixelLINK, Ottowa, ON, Canada). A 10× objective is used. Due to the thickness of the PDMS seal and the limited working distance of the objective, a higher magnification is not possible. For image analysis, SPIP (Image Metrology A/S, Hørsholm, Denmark) is used to obtain cross-sectional plots of the light intensity. Data fitting and statistics on the data are done in Origin Pro 8 (Originlab Cooperation, Northampton, MA, USA). An example of a microscope image, cross-sectional line, and a fitted curve are shown in Fig. 3.

3.3 FEM modeling

To interpret the experimental data, numerical values are obtained by using finite-element-modeling. This is done by utilizing a commercially available software, COMSOL Multiphysics 4.0a (COMSOL AB, Stockholm, Sweden).

A 2D COMSOL model is used to simulate the flow behavior in a microfluidic channel junction. Such a model should be sufficient to describe the entire 3D system due to symmetry in the z-direction. In order to ensure this, a few simulations are run in a full 3D model to investigate the exact flow profiles. In accordance with Nasir et al. (2011), a slightly hourglass-formed profile is obtained in the z-direction. Nasir et al.'s simulations were conducted on a T-junction with only one sheath-flow, but still showed that the shape of the profile depends on both *Re* and angle between channels, where higher *Re* and angle increases the amount of sample-fluid pushed towards top and bottom of the channel. At comparable *Re* the effect is however less pronounced in our 3-channel junction, probably due to the difference in boundary conditions. The 3D simulations are run for three values of r (4, 6, and 9), keeping $\theta = 90°$. Measuring the sample width in the central z-plane yields similar results to the corresponding 2D models with 6% difference for $r = 9$ and slightly higher for decreasing values of r.

The model geometry consists of a 3 mm long channel with two side channels forming a junction 0.5 mm from the inlet end. All channels are 100 μm wide. The geometry is meshed with an ultrafine free triangular mesh (maximum element size 5 μm), resulting in around 40,000 finite elements.

All liquid flow modeling is handled using the "Laminar Flow" package from the MEMS-module. All liquids are modeled as water at room temperature. No-slip boundary conditions are applied to all side-walls. The three inlets (one sample and two side channels) are treated as laminar inflows with a set flow rate and a long entrance length (1 cm) to ensure stable laminar flow. The flow rate in the main channel is fixed at 10 μl/min, while the side channels are varied from 0.1 to 110 μl/min, depending on the desired flow-ratio. The outlet is pressure controlled with a pressure of 0 Pa. The model equations are solved by finding a stationary solution for the velocity field of all flows.

To visualize the hydrodynamic focusing the "Transport of Diluted Species" package is added to the model. All walls are set to no flux and the diffusion constant to 2.2×10^{-11} m^2/s (self-diffusion of water). The velocity field is set to $u(y, z)$ from the previous step in the model. The concentration of the virtual sample liquid is set to 0 at side-channels and output, and 1 mol/m^3 in the input.

After a solution has been obtained, cross sectional plots of the concentration are obtained and treated the same way as those obtained from the CCD images in the experimental section.

4 Results and discussion

4.1 Influence of r on f

The first experiment focuses on investigating how the volumetric flow rates of side (Q_s) and sample (Q_i) fluids influence flow fraction f. This is expressed as a function of the flow-ratio of the system (r). For this purpose a simple hydrodynamic focusing chip is designed (Fig. 2, left). Images are obtained for flow ratios from $r = 0.01$ to $r = 11$, and analyzed. The width of the sample flow w_f is measured at a distance of $x = 500$ μm (see Fig. 1) and is

defined as the full-width-half-max (FWHM) of a Gaussian fit to the peak in a cross-section of the light-intensity of the image (see Fig. 3).

An identical structure has been re-created in COMSOL and using identical parameters for volumetric flow and geometry, the hydrodynamic focusing has been modeled in a 2D cross-sectional view. Data points are obtained by extracting the intensity data of a virtual colored liquid in the sample flow and then calculating the FWHM from a Gaussian curve fit.

Finally, the flow fraction f is calculated for different values of r based on Eq. 9. The results from all three methods are shown in Fig. 4.

A clear correlation between all three sets of data is visible. The behavior of $f(r)$ agrees with the results found by Lee et al. (2006). The focusing fraction f decreases from 0.65 down to 0.10 with increasing values of r (Fig. 4). Obviously, efficient hydrodynamic focusing only occurs for $r > 1$, meaning that the side-channel flow (Q_s) must always be at least equal to or bigger than the sample flow (Q_i), in order to achieve focusing. A non-linear behavior is apparent and shows that for higher values of r, a further increase has little or no influence on the hydrodynamic focusing. At low r however, the effect is quite pronounced.

When comparing the calculated values (based on Eq. 9) with the experimental data and numerical simulations we see fair agreement particularly at higher values of r. The agreement is further off at low r where the side fluid undergoes greater acceleration than assumed in the calculation.

4.2 Influence of θ on f

While the previous experiment confirms a tendency that has been reported in the literature, this section investigates how the geometry of the channel junction affects the hydrodynamic focusing effect. More precisely, how different values of the side- and main-channel angle θ affect the focusing fraction f.

A constant flow ratio of $r = 6$ is selected, mainly because it is sufficiently high to give good focusing and is thereby a realistic value for use in experimental setups. As in the previous section the chip is mounted in a microscope-setup and images of the flow behavior are obtained during focusing in each of the three different channel-junctions (Fig. 2). The images are analyzed using SPIP and Origin Pro 8, and the averaged width of the focused stream w_f is measured at points along the main channel. The measured values are converted to micrometers based on a profilometric measurement of the channel width. The results are plotted in Fig. 5.

A clear tendency to rapid focusing is observed for all three angles. Within 100–200 μm of the junction the width of the sample flow has decreased by a factor of 10 and remains constant thereafter. The close-up on Fig. 5 also reveals that the lowest absolute value for f (0.083) and maximum flow focusing is obtained with the 90° angle design. As θ becomes lower, $f_{\min}$ increases, up to 0.109 for 45°. For all three angles, the minimum value is obtained around 200 μm from the junction. Towards 1,000 μm f increases slightly for all three values of θ. The results are summarized in Table 1.

It is noted that the f value increases with increasing distance from the junction. The effect seems to be slightly increased for the flow that has been focused down to the smallest value. Over the first millimeter the flow width in the 90° side-channel chip increases by 42.7%, while the 45° design only induces a 8.4% increase in width. This long-range behavior will be investigated further in the next section.

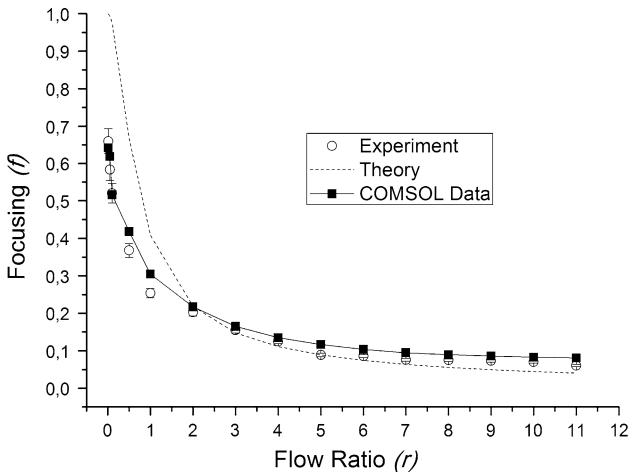

Fig. 4 Focusing fraction f in a 90° junction, data measured as the FWHM of a cross-sectional cut as a function of increasing flow ratios (r). Experimental data, modeled COMSOL data and calculated values are plotted

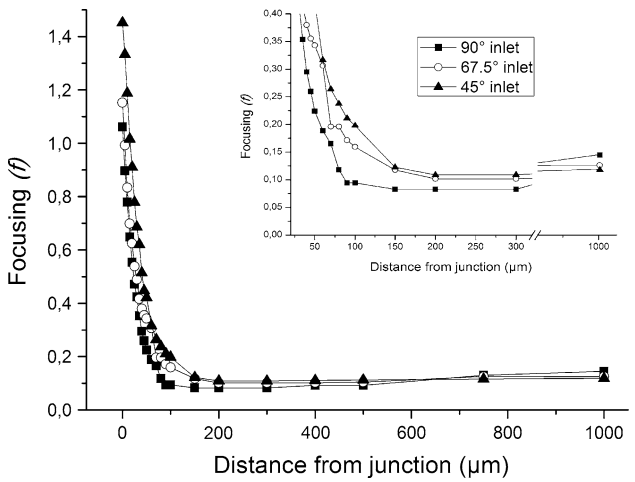

Fig. 5 Focusing fraction f as a function of distance from the junction for $r = 6$, showing the rapid decrease in width along the channel and a stabilization-effect after 100–200 μm. Close-up of the area of particular interest. Shown for three values of θ

Table 1 Focusing fraction f from measured FWHM, for three different angles at different positions along the main-channel

Angle θ	Minimum f	f at 1,000 μm	% increase
90°	0.083	0.145	42.7
67.5°	0.102	0.125	18.4
45°	0.109	0.119	8.4

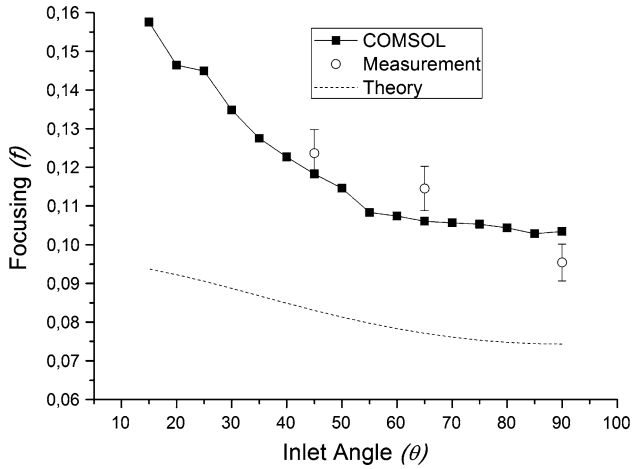

Fig. 6 Focusing fraction f as a function of angle θ between side and sample channels, for $r = 6$, from COMSOL model (*filled squares*). Experimental results (*open circles*) are shown for comparison. Also shown is calculated data based on the modified Bernoulli's equation (*dotted line*)

The influence of the angle on focusing is further investigated using COMSOL modeling. The model used in the previous section is maintained and a parametric sweep of angles between side- and main-channel is added. The flow ratio is maintained at $r = 6$. Focusing fraction f is obtained by using the FWHM value of a Gaussian curve fit of the individual data-sets measured 200 μm from the junction. The results are shown in Fig. 6. The simulations show a steady decrease in the sample flow width as the sheath channel angle is increased toward 90° corresponding to a 55% reduction in f between the smallest and largest angle. The three experimental points obtained at this value of r would seem to agree reasonably well with these simulations.

The simple theoretical model introduced in Eq. 9 to calculate f (Theory curve in Fig. 6) produces poor correlation with the numerical simulation and experiment. As discussed previously this model does introduce a number of simplifications. Perhaps most notably it takes no account of 3D behavior such as the hourglass profiles discussed in Nasir et al. (2011). Such a profile would certainly increase the apparent width of the focusing as seen through top-down imaging and would explain the discrepancy of the calculated with the observed width. It cannot however account for the discrepancy between the calculation using Eq. 9 and the COMSOL model which is also 2D and produces a closer fit to the data. It is more likely that another assumption such as that of a flat velocity profile across the channels is responsible for the difference. Nevertheless the trend given by the simple equation is quite similar to the COMSOL model and suggests that the the pressure due to redirection of the sheath flows is a factor in determining the short range focusing behavior.

4.3 Long-range flow behavior

The previous section indicates that the angle of the sheath streams has an influence on focusing. Clearly a sheath angle of 90° produces the biggest reduction in the sample stream width immediately after the junction. However they also show in Fig. 5 that the degree of focusing further along the channel varies for the different angles. In order to investigate this, the focusing fraction f is measured along a 1 cm long channel for two different angles ($\theta = 45°$ and $\theta = 90°$). The measurements are replicated on three different chips (three for each angle) in order to eliminate random variation due to the production method. The influence of r is also investigated for values of $r = 3, 6, 10$, as they result in a spread of focus widths (see Fig. 4).

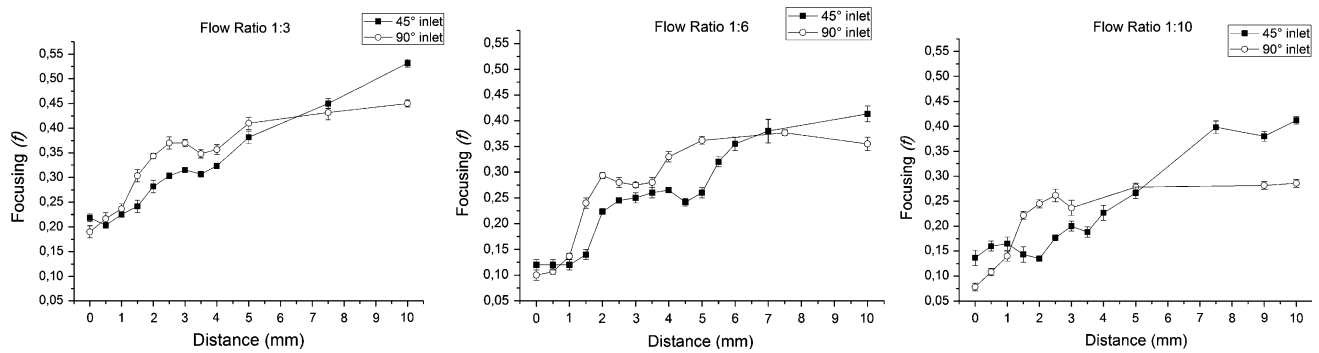

Fig. 7 Focusing fraction f along the channel for both 45° and 90° side-channel angles

Images are obtained for all three values of r, and for both angles, along the 10 mm of the main channel. Mean values for f are plotted in Fig. 7, with error bars indicating the sample standard deviation of all three measurements. The tendency observed in the previous experiment is consistent with the one observed in this experiment, at all three values for r. The measurements indicate that f is considerably smaller for $\theta = 45°$ for a wide range of distances, for all three values of r. In all three series of measurements the data support the previous results (Sect. 4.2), where the minimum value of f is found near the junction and in the perpendicular design (design 18). At the far end of the channel there is a crossover and the perpendicular design again provides the best focusing (smallest f). The region of interest is however the one ranging from 1 to 5 mm, where a previously unreported effect occurs.

Nasir et al. (2011) have shown that *Re* have an important influence on the streamlines in a fluid-junction, where lower *Re* values gives a very flat concentration distribution along the channel and increasing *Re* gives rise to similar effects as those observed here. This is because at higher flow rates (and hence higher *Re*) side flows posses a higher momentum and hence gives rise to similar higher inertia change as described earlier in this paper. In this series of experiments, however, *Re* is kept constant for the different geometries and the effect cannot be ascribed to the *Re* alone. The slight hour-glass shape of the focused stream observed by Nasir et al. and also reproduced in our 3D COMSOL models, can account for some of the observed divergence of the flow, though not entirely, as only a less percentage of increase in width is obtained when taking this effect into account.

To estimate the influence of diffusion on our measurements, the average diffusion length for a typical food dye molecule is calculated ($D = 2 \times 10^{10}$ m^2/s, Inglesby 2001). Across the entire channel length of 10 mm using typical flow rates, the diffusion length is in the range of 4.5 μm or lower depending on r.

The effect of the slight hourglass shape combined with the diffusion of the color molecules are however not enough to explain the phenomenon. Furthermore, both these should result in a linear increase of f with distance and can hence not explain the dips observed in the curves.

The long-range behavior of the focused flow can however be attributed to a Venturi-like effect, where the tighter focus (smaller f) of the 90° design gives rise to a bigger pressure gradient across the channel. When this pressure is equalized a slight expansion of the sample flow is observed. This is also evident for higher flow ratios, where the range in which the angle-depending divergence occurs is shorter (around 4 mm for $r = 10$, while it is almost 6 mm for $r = 3$). This is due to the bigger difference in f and hence velocities between side and sample flows. The extra pressure term ascribed to the bending flow during focusing also explains why the effect is transitory in that the excess pressure will dissipate once the sheath flow has turned the corner. To investigate this effect further, pressure-curves are obtained from the 2D COMSOL model for both 45° and 90° designs. These are plotted in Fig. 8. As the plots are obtained just after junction a slightly higher pressure in the 90° structure is evident (see Eq. 5). Furthermore, the aforementioned pressure gradient across side and core flow is observed and is indeed higher for the 90° design. Further along the channel the pressure equalizes and the curves flatten out (not shown) as is also suggested by the experimental data.

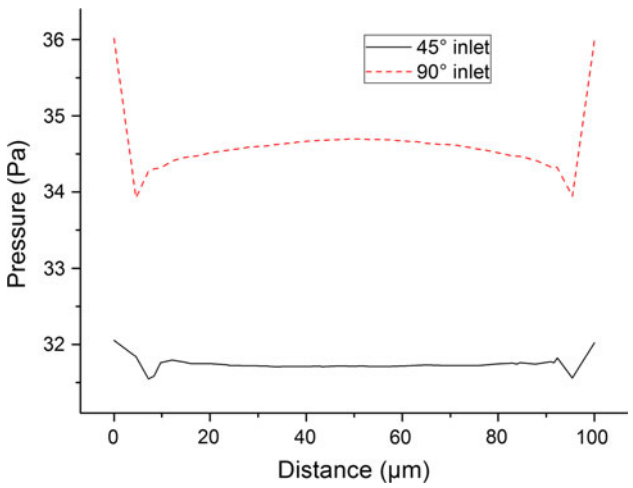

Fig. 8 Pressure profiles across the main channel immediately after the junction. COMSOL data

5 Conclusion

In this paper the influence on hydrodynamic focusing of flow ratio between sample and sheath flows is investigated. Both experimental, modeled and calculated data indicate that a higher flow ratio produces a narrower focused stream. Furthermore, we show that the dependence is non-linear. For low flow ratio values, the dependence is almost exponential, while at higher values, very low influence is observed.

This paper also shows that the local geometry of the channel-junction in a microfluidic device influences the hydrodynamic focusing. Experimental results, modeled data and calculated values show that the angle between side- and main-channels influences the minimum focusing width close to the junction, and that a perpendicular junction provides the smallest width. This effect is ascribed to an additional pressure term resulting from the change in direction of the sheath flows.

Further investigation of the angle dependence also indicates that for certain distances along the main channel, a 45° design results in a narrower steam than a 90° design. This can be attributed to a combination of effects. In particular we attribute this to Venturi-effect-like behavior caused by the difference in flow widths giving rise to pressure variation across the channels. With the current experimental method however, this effect is difficult to separate from the effect of diffusion and 3D changes in the flow cross-sections. Further investigations using 3D imaging methods are needed to confirm this effect.

These results are quite significant since it is often of interest in lab-on-a-chip systems to utilize the entire length of the chip for different measurements or further flow processing, and hence one has to be aware of the fact that the effective size of the measurement volume might change along the channel.

Acknowledgments The authors gratefully acknowledge the financial support provided from the European Union's Fund for Regional Development (EFRU) through the InterReg 4A project "Lab-on-a-chip technique for quality-control in food- and bio-industry".

References

Blankenstein G, Larsen UD (1998) Modular concept of a laboratory on a chip for chemical and biochemical analysis. Biosens Bioelectron 13(3–4):427

Crosland-Taylor PJ (1953) A device for counting small particles suspended in a fluid through a tube. Nature 171(4340):37

de Mello AJ, Edel JB (2007) Hydrodynamic focusing in microstructures: improved detection efficiencies in subfemtoliter probe volumes. J Appl Phys 101(8):084903. doi:10.1063/1.2721752

Fu LM, Yang RJ, Lin CH, Pan YJ, Lee GB (2004) Electrokinetically driven micro flow cytometers with integrated fiber optics for on-line cell/particle detection. Anal Chim Acta 507(1):163. doi:10.1016/j.aca.2003.10.028

Garstecki P, Gitlin I, DiLuzio W, Whitesides GM, Kumacheva E, Stone HA (2004) Formation of monodisperse bubbles in a microfluidic flow-focusing device. Appl Phys Lett 85(13):2649. doi:10.1063/1.1796526

Gobby D, Angeli P, Gavriilidis A (2001) Mixing characteristics of T-type microfluidic mixers. J Micromech Microeng 11(2):126. doi:10.1088/0960-1317/11/2/307

Godin J, Chen CH, Cho SH, Qiao W, Tsai F, Lo YH (2008) Microfluidics and photonics for bio-system-on-a-chip: a review of advancements in technology towards a microfluidic flow cytometry chip. J Biophoton 1(5):355. doi:10.1002/jbio.200810018

Hertzog DE, Michalet X, Jager M, Kong XX, Santiago JG, Weiss S, Bakajin O (2004) Microchip flow cytometry using electrokinetic focusing. Anal Chem 76(24):7169. doi:10.1021/ac048661s

Howell PB, Golden JP, Hilliard LR, Erickson JS, Mott DR, Ligler FS (2008) Two simple and rugged designs for creating microfluidic sheath flow. Lab Chip 8(7):1097. doi:10.1039/b719381e

Huh D, Tung YC, Wei HH, Grotberg JB, Skerlos SJ, Kurabayashi K, Takayama S (2002) Use of air-liquid two-phase flow in hydrophobic microfluidic channels for disposable flow cytometers. Biomed Microdevices 4(2):141

Huh D, Gu W, Kamotani Y, Grotberg JB, Takayama S (2005) Microfluidics for flow cytometric analysis of cells and particles. Physiol Meas 26(3):R73. doi:10.1088/0967-3334/26/3/R02

Inglesby MK, Zeronian SH (2001) Diffusion coefficients for direct dyes in aqueous and polar aprotic solvents by the NMR pulsed-field gradient technique. Dyes Pigments 50(1):3. doi:10.1016/S0143-7208(01)00035-3

Knight JB, Vishwanath A, Brody JP, Austin RH (1998) Hydrodynamic focusing on a silicon chip: mixing nanoliters in microseconds. Phys Rev Lett 80(17):3863

Lee GB, Hung CI, Ke BJ, Huang GR, Hwei BH (2001) The hydrodynamic focusing effect inside rectangular microchannels. J Micromech Microeng 11(5):567

Lee GB, Chang CC, Huang SB, Yang RJ (2006) The hydrodynamic focusing effect inside rectangular microchannels. J Micromech Microeng 16(5):1024. doi:10.1088/0960-1317/16/5/020

Lin CH, Lee GB (2003) The hydrodynamic focusing effect inside rectangular microchannels. J Micromech Microeng 13(3):447

Mao XL, Waldeisen JR, Juluri BK, Huang TJ (2007) Hydrodynamically tunable optofluidic cylindrical microlens. Lab Chip 7(10):1303. doi:10.1039/b708863a

Martin-Banderas L, Flores-Mosquera M, Riesco-Chueca P, Rodriguez-Gil A, Cebolla A, Chavez S, Ganan-Calvo AM (2005) Flow focusing: a versatile technology to produce size-controlled and specific-morphology microparticles. Small 1(7):688. doi:10.1002/smll.200500087

Nasir M, Mott DR, Kennedy MJ, Golden JP, Ligler FS (2011) Parameters affecting the shape of a hydrodynamically focused stream. Microfluid Nanofluid 11(2):119. doi:10.1007/s10404-011-0778-5

Pollack L, Tate MW, Darnton NC, Knight JB, Gruner SM, Eaton WA, Austin RH (1999) Compactness of the denatured state of a fast-folding protein measured by submillisecond small-angle x-ray scattering. Proc Natl Acad Sci USA 96(18):10115

Regenberg B, Kruhne U, Beyer M, Pedersen LH, Simon M, Thomas ORT, Nielsen J, Ahl T (2004) Use of laminar flow patterning for miniaturised biochemical assays. Lab Chip 4(6):654. doi:10.1039/b409141h

Schrum DP, Culbertson CT, Jacobson SC, Ramsey JM (1999) Femtomole mixer for microsecond kinetic studies of protein folding. Anal Chem 71(19):4173

Spielman L, Goren SL (1968) Improving resolution in coulter counting by hydrodynamic focusing. J Colloid Interface Sci 26(2):175

Stone HA, Stroock AD, Ajdari A (2004) Engineering flows in small devices: microfluidics toward a lab-on-a-chip. Annu Rev Fluid Mech 36:381. doi:10.1146/annurev.fluid.36.050802.122124

Squires TM, Quake SR (2005) Microfluidics: fluid physics at the nanoliter scale. Rev Modern Phys 77(3):977

Sundararajan N, Pio MS, Lee LP, Berlin AA (2004) Three-dimensional hydrodynamic focusing in polydimethylsiloxane (PDMS) microchannels. J Microelectromech Syst 13(4):559. doi:10.1109/JMEMS.2004.832196

Takayama S, McDonald JC, Ostuni E, Liang MN, Kenis PJA, Ismagilov RF, Whitesides GM (1999) Compactness of the denatured state of a fast-folding protein measured by submillisecond small-angle x-ray scattering. Proc Natl Acad Sci USA 96(10):5545

Takeuchi S, Garstecki P, Weibel DB, Whitesides GM (2005) An axisymmetric flow-focusing microfluidic device. Adv Mater 17(8):1067. doi:10.1002/adma.200401738

Vilkner T, Janasek D, Manz A (2004) Micro total analysis systems. Recent developments. Anal Chem 76(12):3373. doi:10.1021/ac040063q

Whitesides GM, Stroock AD (2001) Flexible methods for microfluidics. Phys Today 54(6):42

Wong PK, Lee YK, Ho CM (2003) Deformation of DNA molecules by hydrodynamic focusing. J Fluid Mech 497:55

Yang J, Pi X, Zhang L, Liu X, Yang J, Cao Y, Zhang W, Zheng X (2007) Diffusion characteristics of a T-type microchannel with different configurations and inlet angles. Anal Sci 23(6):697. doi:10.2116/analsci.23.697

Zhe J, Jagtiani A, Dutta P, Hu J, Carletta J (2007) A micromachined high throughput Coulter counter for bioparticle detection and counting. J Micromech Microeng 17(2):304. doi:10.1088/0960-1317/17/2/017